Optical properties of $Pr_{0.5}Ca_{0.5}CoO_3$ single crystal

2008 J. Phys.: Condens. Matter 20 055222

(http://iopscience.iop.org/0953-8984/20/5/055222)

J. Phys.: Condens. Matter **20** (2008) 055222 (5pp) doi:10.1088/0953-8984/20/5/055222

Optical properties of $Pr_{0.5}Ca_{0.5}CoO_3$ single crystal

J Zhou, P Zheng and N L Wang[1]

Beijing National Laboratory for Condensed Matter Physics, Institute of Physics, Chinese Academy of Sciences, Beijing 100080, People's Republic of China

E-mail: nlwang@aphy.iphy.ac.cn

Received 17 October 2007, in final form 18 December 2007
Published 18 January 2008
Online at stacks.iop.org/JPhysCM/20/055222

Abstract

We report on a temperature-dependent optical study on the carrier dynamics of a perovskite cobalt oxide $Pr_{0.5}Ca_{0.5}CoO_3$. The single crystal samples, grown from a floating zone furnace and post-annealed under high oxygen pressure, show a sharp metal–insulator transition near 90 K. At high temperature, we observe an overall metallic response due to the band conduction of Co e_g electrons, but a localization effect is found at low frequencies. With decreasing temperature, a transfer of spectral weight to high frequencies is seen and a small energy gap of about 60–70 cm^{-1} is formed. We elaborate that the spectral evolution could be well understood from the reconstruction of Co 3d bands associated with spin state transition and charge ordering.

(Some figures in this article are in colour only in the electronic version)

1. Introduction

The transition metal cobalt oxides have attracted much attention in the condensed matter community because they show a diversity of interesting physical properties. The superconductivity discovered in layered hydrated Na_xCoO_2 is one example. The spin state transition of Co^{3+} ion in perovskite-related cobalt oxides is another very interesting phenomenon [1, 2]. With a change of temperature, or pressure or carrier concentration, the spin state of Co^{3+} may be changed from the low spin state (LS, $t_{2g}^6e_g^0$, $S = 0$) to the intermediate state (IS, $t_{2g}^5e_g^1$, $S = 1$) or the high spin state (HS, $t_{2g}^4e_g^2$, $S = 2$) [3–13]. The existence of such phenomenon indicates that the energy difference between the crystal field splitting $10Dq$ and Hund's coupling energy J_H in CoO_6 octahedral is rather small. Accompanied with a spin state transition (SST), the compounds usually exhibit a metal–insulator transition (MIT). The broad studied examples are $LaCoO_3$ and $LnBaCo_2O_{5+\delta}$ (Ln = Pr, Nd, Sm, Eu, Gd and Tb) ($0 \leqslant \delta \leqslant 1$), where MITs are found in both systems. The difference is that it is a thermal excitation in $LaCoO_3$ and it is a first-order phase transition in $LnBaCo_2O_{5+\delta}$. So it is a more abrupt process in the later.

Element substitutions are widely used to tune the crystal field splitting as they can change the volume of the CoO_6 octahedral or the Co–O–Co angle. In the study of the $R_{1-x}A_xCoO_3$ (R = Y, and various rare earth elements, A = Ba, Sr, and Ca), Tsubouch *et al* found an abrupt MIT near 90 K with decreasing temperature in $Pr_{1-x}Ca_xCoO_3$ at a very narrow Ca region $x \sim 0.5$ [9, 11], similar to those found in $LnBaCo_2O_{5+\delta}$. A further transition to long-range ferromagnetic order appears at 2 K. Due to a $GdFeO_3$-type distortion, the Co–O–Co bond angle in CoO_6 octahedral decreases as much as 4° when the temperature reduces from 297 to 10 K [9]. It enlarges the splitting of the crystal field. The primary origin of the MIT was thought to be the appearance/disappearance of e_g electrons due to the change of the spin state of Co^{3+} from the intermediate state to the low spin state. Then the Co^{3+} and Co^{4+} both stayed in the low spin states (t_{2g}^6 and t_{2g}^5). Fujita *et al* made extensive studies on $R_{1-x}A_xCoO_3$ and found that the sharp MIT occurs only for (R, A) = (Pr, Ca) with x close to 0.5 [14, 15]. In addition, the metal–insulator transition temperature is sensitive to the sample's heat treatment conditions [16].

So far, all available experimental studies, including structural, transport, and magnetic investigations, on $Pr_{0.5}Ca_{0.5}CoO_3$ have been performed on polycrystalline samples. Infrared optical spectroscopy is a powerful bulk-sensitive tool to explore the electronic structure and carrier dynamics. The technique has not been employed to this system due to the unavailability of single crystal samples. Recently we successfully grew the single crystals of $Pr_{0.5}Ca_{0.5}CoO_3$ by the floating

[1] Author to whom any correspondence should be addressed.

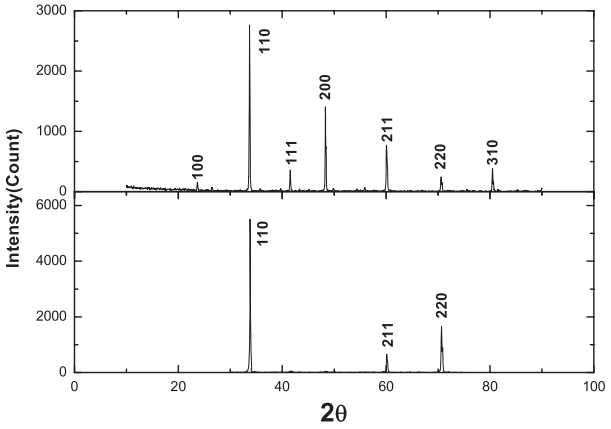

Figure 1. Powder XRD (top panel) and single crystal XRD (bottom panel) for $Pr_{0.5}Ca_{0.5}CoO_3$ single crystals.

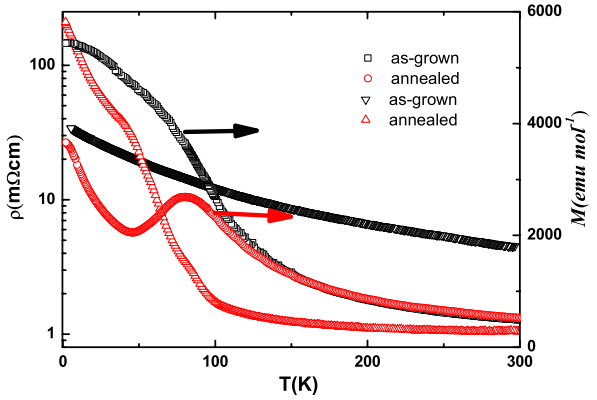

Figure 2. The dc resistivity and the dc magnetizations under 5 T magnetic field versus temperature for $Pr_{0.5}Ca_{0.5}CoO_3$.

zone method. After being annealed under high oxygen pressure, we observed a metal–insulator transition similar to that found in polycrystalline compound. In this work, we first report the growth and characterizations of single crystals, then present a detailed optical investigation on the charge dynamics across the MIT in order to shed further light on the origin of the MIT.

2. Crystal growth and characterizations

The $Pr_{0.5}Ca_{0.5}CoO_3$ single crystal was grown from a floating zone optical image furnace. The polycrystalline samples were prepared first from the mixture of Pr_6O_{11}, $CaCO_3$, and Co_3O_4, in the same solid-state reaction method as that introduced in [9]. The calcinated powders were already in a single phase from the x-ray diffraction measurement. Then the powders were pressed into a 8 mm diameter $\times 9$ cm long rod under a pressure of 50 MPa and annealed at 1200 °C for a day under the oxygen atmosphere. About 2 cm of the rod was cut as seed. The rest was taken as feed rod and pre-melted in the floating zone furnace with a feeding speed of 10 mm h^{-1}. The obtained pre-melted rod was used again as a feed and re-melted with a much slower feeding speed 0.4 mm h^{-1} under 7.5 atm oxygen pressures. During the procedures, the feed rod and seed were rotated in contrary directions at a speed of 20 rpm to insure a uniform melting zone.

X-ray diffraction (XRD) with Cu Kα_1 ($\lambda = 1.54056$ Å) radiation was used to examine the phase of the as-grown crystal. A piece of crystal was cut from the as-grown crystal rod and ground into powders. The XRD measurement on those powders confirms the single phase of the $Pr_{0.5}Ca_{0.5}CoO_3$ crystal, as shown in the upper panel of figure 1. A direct XRD measurement on the as-grown crystal along the growth direction shows that the major peaks are from (110) diffractions (bottom panel of figure 1), indicating that the crystal growth is essentially along a direction about 45° relative to the *a*- or *b*-axis.

The dc resistivity $\rho(T)$ (by a standard four-probe method) and the field-cooling dc magnetization $M(T)$ under a 5 T magnetic field were measured in a Quantum Design physical property measurement system (PPMS). The as-grown crystal shows a semiconducting-like $\rho(T)$ without showing any abrupt change. The dc magnetization shows a Curie–Weiss-like behavior, though a deviation from Curie–Weiss dependence becomes evident at low T. As is known from the study of the polycrystalline samples, the sharp MIT can be achieved when the samples were annealed in high oxygen pressure. So, we annealed the as-grown crystals under high oxygen pressure in a HPS-5015E furnace from Morris Research Inc. The $\rho(T)$ and $M(T)$ curves for a sample annealed at 600 °C for 48 h under oxygen pressure of 170 bars are displayed in figure 2. Then the resistivity at high temperature is reduced significantly, and a prominent upturn emerges roughly below 100 K, which could be defined as the MIT temperature T_{MI}. But even above T_{MI}, $\rho(T)$ curve also has a negative slope, suggesting a non-metallic nature. It can be seen quite often in transitional metal oxides for which the mean free path of electrons might be close to the lattice constant. The dc magnetization under a 5 T magnetic field show a sharp decrease near 77 K, a temperature corresponding to the mid-point of the sharp increases of dc resistivity. Those curves are similar to the data reported in [16] for polycrystalline samples. The MIT appears broader than that obtained for polycrystalline samples. We attribute this to the inhomogeneity induced by the process of annealing oxygen into the denser single crystal.

3. Optical spectroscopy measurement and analysis

Optical measurements were performed on the high oxygen pressure annealed crystal showing the sharp MIT. The crystal, whose surface being cut perpendicular to the growth direction, was finely polished. The near-normal incident reflectance was measured from a Bruker 66 v/s spectrometer in the frequency range from 40 to 25 000 cm^{-1} and from a grating spectrometer from 25 000 to 50 000 cm^{-1}, respectively. An *in situ* overcoating technique was employed for reflectance measurements [17]. We performed Kramers–Kronig transformation of $R(\omega)$ to obtain the optical conductivity spectra. For the low frequency extrapolation, we use constant and Hagen–Rubens relation. At high frequency side, above the maximum frequency in the data file, the

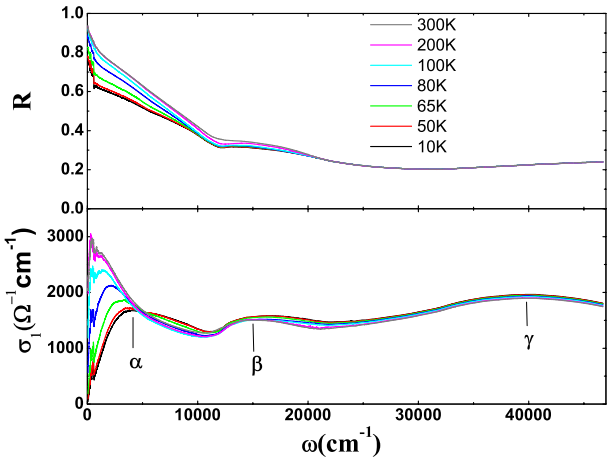

Figure 3. Temperature dependence of the reflectivity spectra (top panel) and optical conductivity spectra (bottom panel) for a $Pr_{0.5}Ca_{0.5}CoO_3$ single crystal.

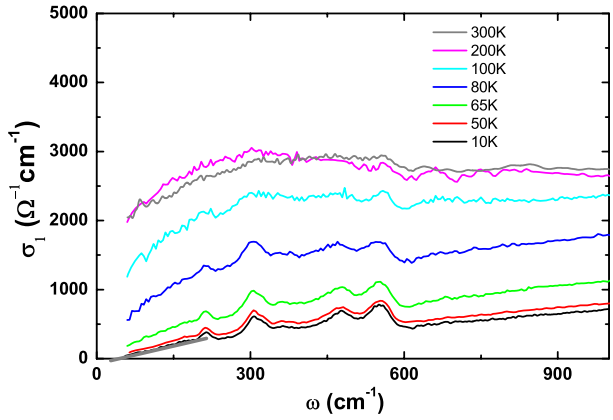

Figure 4. Temperature dependence of optical conductivity spectra in the low energy region (0–1000 cm^{-1}). A gray straight line near the left bottom is the linear extrapolation of the low frequency conductivity for the estimation of the gap.

reflectance is extrapolated as ω^{-1} up to 100 000 cm^{-1} followed by a function of ω^{-4}.

Figure 3(a) shows the reflectance spectra taken at various temperatures below 47 000 cm^{-1}. In accord with the non-metallic dc resistivity behavior with a negative slope, we find that the low frequency reflectance decreases with decreasing temperature. The main spectral change caused by temperature variation is roughly below 20 000 cm^{-1}. As the temperature is decreased below T_{MI}, the low frequency reflectance shows a rapid decrease, a trend expected for a typical insulating compound. In addition, sharp infrared phonon structures become prominent in the far-infrared region.

Figure 3(b) shows the spectra of the optical conductivity $\sigma_1(\omega)$ at different temperatures. Strong temperature dependence is seen at low frequencies. At room temperature, the conductivity below 10 000 cm^{-1} shows an overall increasing behavior with decreasing ω, i.e. a Drude-like response. However, the conductivity drops at very low frequency, roughly below 300 cm^{-1} (see figure 4). This drop is usually considered as a signature of charge localization. Thus the low-ω data demonstrate the non-metallic nature of the sample. When the temperature decreases below 100 K, the low energy component is severely suppressed. A small gap could be identified in the conductivity curve as we shall show later. The missing spectral weight is transferred to higher energies, forming a peak α. The center of α shifts from about 2000 to 4000 cm^{-1} as the temperature is lowered down from 100 to 10 K. At higher energies, there are two noticeable peaks in the conductivity spectra, which we labeled as β and γ, respectively. The two peaks are present in both the metallic and insulating states. The β peak shifts slightly, roughly from 15 000 to 16 500 cm^{-1}, as the temperature deceases. The position of the γ peak, centered near 40 000 cm^{-1} (5 eV), is temperature independent.

The optical conductivity spectra in the expanded frequency region (0–1000 cm^{-1}) are shown in figure 4. Although the conductivity shows a drop below about 300 cm^{-1} at high temperature, which was assigned to carrier localization effect, the value at zero-frequency limit is apparently finite. There is no gap opening at high T. However, at low temperature (below T_{MI}), the conductivity is severely suppressed, leading to the formation of a gap. An linear extrapolation of the conductivity spectrum at low frequency indicates that the gap value is rather small, only about 60–70 cm^{-1} at 10 K. With the removal of the electronic contribution, the phonon peaks become prominent at low T.

Understanding the above spectral change, particularly the origin of the small gap and the variation of the peak α, is the main task of this work, which is also crucial for understanding the change of electronic structure across the MIT in $Pr_{0.5}Ca_{0.5}CoO_3$. Considering the fact that the partially filled 4f states of Pr are more readily localized, we only need to take account of the Co 3d bands, which are split into e_g and t_{2g} bands due to the octahedral crystal field splitting [18]. The states near the Fermi level would be dominated by the Co 3d bands (some hybridizations with O 2p character exist). Thus the MIT and accompanied changes are mainly due to the variation of the 3d electronic states in transitional metal cobalt.

At high temperature, all Co ions have equivalent positions in the structure. The valence state of Co is $Co^{3.5+}$. There are 5.5 electrons in the d orbitals, thus the Co 3d bands are partially filled. It has been accepted that the configuration $t_{2g}^5e_g^{0.5}$ exists in $Pr_{0.5}Ca_{0.5}CoO_3$ at high temperatures. Partially filled t_{2g} and e_g bands, being hybridized with O 2p band, cross the Fermi level (there is still no conclusion whether or not the t_{2g} band crosses the Fermi level, but here we take the idea that it crosses the Fermi level but has less contribution to electronic conduction than e_g band), leading to an *intraband* transition at low frequencies [13, 19–21]. Except that, an *interband* transition exists between Co t_{2g} and e_g bands. This should induce the β peak. Its energy scale is also comparable to the band calculations for $HoCoO_3$ and $LaCoO_3$ (the energies between t_{2g} and e_g band are 2.04 eV and 1.93 eV, respectively) [22]. The γ peak would correspond to the *interband* transition between O 2p states and Co e_g states, which is consistent with the ARPES (angle-resolved photoemission spectroscopy) results [22]. In this case, the

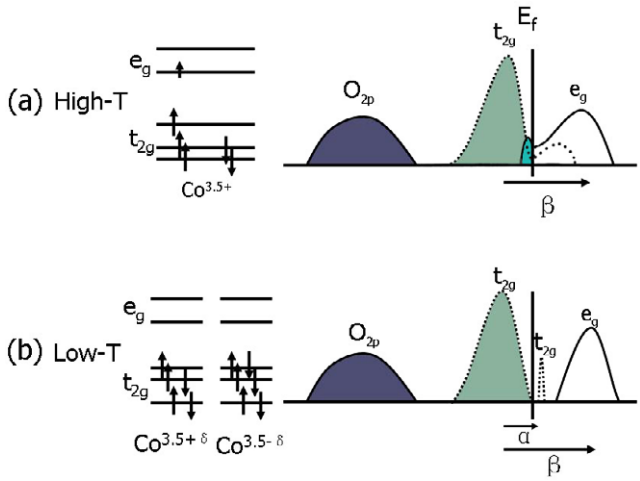

Figure 5. Schematic diagram of the electronic states above and below the MIT temperature. (a) Above T_{MI}, there is only one equivalent position for Co in the structure with a valence state of $Co^{3.5+}$. Both the Co e_g and t_{2g} bands are partially filled, leading to a low frequency *intraband* transition. β represents an *interband* transition from occupied part of Co t_{2g} to unoccupied part of e_g bands. (b) Below T_{MI}, the spin-up Co e_g electrons reverse to spin down through the SST and the states of Co become $Co^{3.5-\delta}$ and $Co^{3.5+\delta}$. The charge and orbital ordering splits t_{2g} bands into two parts, forming a gap. A new *interband* transition α appears between split t_{2g} bands.

electronic state above T_{MI} could be understood from the schematic diagram of figure 5(a).

When the temperature decreases below T_{MI}, the crystal field splitting between t_{2g} and e_g band increases and e_g electrons jump to t_{2g} energy levels leading to the SST. The SST naturally accounts for the sudden drop in the dc magnetization or spin susceptibility. However, as there will be 5.5 electrons in the t_{2g} levels, the compound could only be a metal unless some other mechanisms working here to open up a gap. In the following we shall discuss the possibilities of SST with simultaneous occurrence of charge ordering and orbital ordering.

In fact, charge ordering exists extensively in Co oxides [23–25]. For example, in $LnBaCo_2O_{5+\delta}$ ($\delta = 1$) which possesses the same electronic configuration of half t_{2g}^5 and half t_{2g}^6, the spin state of Co^{3+} changes from the intermediate spin state to the low spin state and the Co^{3+} and Co^{4+} get ordered as the temperature drops below T_{MI}. This could also happen to $Pr_{0.5}Ca_{0.5}CoO_3$. In this situation, the electrons at the Co^{3+} and Co^{4+} sites are localized and a splitting of the t_{2g} band into higher and lower parts would occur, opening a charge-density-wave-like gap. This can easily explain the experimental phenomena: both SST and MIT. The charge ordering requires two inequivalent positions of Co. Tsubouchi *et al* performed neutron diffraction experiments on polycrystalline $Pr_{0.5}Ca_{0.5}CoO_3$, but could not resolve inequivalent Co sites [9], although they also proposed localized Co^{3+} and Co^{4+} in the low temperature phase. We notice that the MIT and the structure distortions in $Pr_{0.5}Ca_{0.5}CoO_3$ are very similar to that found in $NdNiO_3$. $NdNiO_3$ crystallizes in the orthorhombically distorted perovskite structure $Pbnm$. It has one e_g electron on each Ni ion, and displays an insulator behavior after MIT. When MIT occurs, the most prominent phenomena are change of the Ni–O–Ni bond angle and the cell volume, like what we described above in $Pr_{0.5}Ca_{0.5}CoO_3$. The available neutron diffraction experiment could not detect inequivalent Ni sites at low temperature [26]. On the contrary, a charge-ordered state, i.e. a small charge disproportionation, in $NdNiO_3$ was resolved by resonant x-ray scattering recently [27–29]. We speculate that the same situation would occur in $Pr_{0.5}Ca_{0.5}CoO_3$. The states of Co^{3+} and Co^{4+} might be $Co^{3.5-\delta}$ and $Co^{3.5+\delta}$ with very small value of δ. But the actual orbital occupation of $Co^{3.5-\delta}$ and $Co^{3.5+\delta}$ is close to t_{2g}^6 and t_{2g}^5. Such a charge ordering state with small difference in the valence state but large difference in the orbital occupations have been well established in magnetite Fe_3O_4 [30, 31]. Note that the actual occupations of t_{2g} orbitals depend on structural distortions. As the low-T structural data indicate a $GdFeO_3$-type distortion where the neighboring CoO_6 octahedrons tilt in different directions, a simultaneous orbital ordering is likely to occur [32–34]. We would like to remark that our optical experiments can not directly probe the charge or orbital ordering, but such a picture provides natural explanation for the gap formation and the spectral evolution. Apparently, further direct experimental probes, e.g. the resonant x-ray scattering experiment, are needed for confirmation.

From the above discussions, the sharp metal–insulator transition and the drop of the spin susceptibility could be well explained by the simultaneous occurrence of SST, charge ordering and even orbital ordering. As illustrated in the schematic band structure picture of figure 5(b), the transfer of the spectral weight from very low energy to higher energy above the α peak, or the formation of the small energy gap, can be naturally assigned to the interband transition of electrons from the lower occupied Co t_{2g} to upper t_{2g} subband. The shift of β peak to high frequencies as the temperature decreases implies the enlarged splitting between Co t_{2g} and e_g band, which is in accord with the prediction.

4. Conclusions

We have grown the $Pr_{0.5}Ca_{0.5}CoO_3$ single crystal and investigated its optical conductivity spectra. At high temperature, we observe an overall metallic response mainly due to the band conduction of Co e_g electrons, but a localization effect is found at low frequencies. With decreasing temperature, a transfer of spectra weight to high frequencies is seen and a small energy gap of about 60–70 cm^{-1} is formed. The MIT in $Pr_{0.5}Ca_{0.5}CoO_3$ is caused by the reconstruction of Co 3d bands associated with SST and charge ordering. We attribute the α peak to the interband transition of electrons within the split Co t_{2g} bands. The β and γ component are due to the transitions from the occupied Co t_{2g} and O 2p to the empty Co e_g bands, respectively.

References

[1] Yamaguchi S, Okimoto Y and Tokura Y 1997 *Phys. Rev.* B **55** R8666
[2] Zhuang M, Zhang W and Ming N 1998 *Phys. Rev.* B **57** 10705

[3] Senaris-Rodriguez M A and Goodenough J B 1995 *J. Solid State. Chem.* **116** 224
[4] Yamaguchi S, Okimoto Y and Tokura Y 1996 *Phys. Rev.* B **54** R11022
[5] Korotin M A, Ezhov S Yu, Solovyev I V and Anisimov V I 1996 *Phys. Rev.* B **54** 5309
[6] Moritomo Y, Akimoto T, Takeo M, Machida A, Nishibori E, Takata M, Sakata M, Ohoyama K and Nakamura A 2000 *Phys. Rev.* B **61** R13325
[7] Fauth F, Suard E and Caignaert V 2002 *Phys. Rev.* B **65** 060401
[8] Frontera C, Garca-Munoz J L, Llobet A and Aranda M A G 2002 *Phys. Rev.* B **65** 180405
[9] Tsubouchi S, Kymen T, Itoh M, Ganguly P, Oguni M, Shimojo Y, Morii Y and Ishii Y 2002 *Phys. Rev.* B **66** 052418
[10] Zhang Q and Zhang W 2002 *Phys. Rev.* B **67** 094436
[11] Tsubouchi S, Kyõmen Tõru and Itoh M 2004 *Phys. Rev.* B **69** 144406
[12] Roy S, Dubenko I S, Khan M, Condon E M, Craig J and Ali N 2005 *Phys. Rev.* B **71** 024419
[13] Takubo K, Son J Y, Mizokawa T, Soda M and Sato M 2006 *Phys. Rev.* B **73** 075102
[14] Masuda H, Fujita T, Miyashita T, Soda M, Yasui Y, Kobayashi Y and Sato M 2003 *J. Phys. Soc. Japan* **72** 873
[15] Fujita T, Miyashita T, Yasui Y, Kobayashi Y, Sato M, Nishibori E, Sakata M, Shimojo Y, Igawa N, Ishii Y, Kakurai K, Adachi T i, Ohishi Y and Takata M 2004 *J. Phys. Soc. Japan* **73** 1987
[16] Luo X G, Li X, Wang G Y, Wu G and Chen X H 2005 *Preprint* cond-mat/0509533
[17] Homes C C, Reedyk M, Crandles D A and Timusk T 1993 *Appl. Opt.* **32** 2976
[18] Flavell W R, Thomas A G, Tsoutsou D, Mallick A K, North M, Seddon E A, Cacho C, Malins A E R, Patel S, Stockbauer R L, Kurtz R L, Sprunger P T, Barilo S N, Shiryaev S V and Bychkov G L 2004 *Phys. Rev.* B **70** 224427
[19] Wu H 2000 *Phys. Rev.* B **62** R11953
[20] Wu H 2001 *Phys. Rev.* B **64** 092413
[21] Wu H 2003 *J. Phys.: Condens. Matter* **15** 503
[22] Nekrasov I A, Streltsov S V, Korotin M A and Anisimov V I 2003 *Phys. Rev.* B **68** 235113
[23] Saitoh T, Yamashita Y, Todoroki N, Kyômen T, Itoh M, Higashiguchi M, Nakatake M and Shimada K 2005 *J. Electron Spectrosc. Relat. Phenom.* **144** 893
[24] Troyanchuk I O, Kasper N V and Khalyavin D D 1998 *Phys. Rev. Lett.* **80** 3380
[25] Suard E, Fauth F, Caignaert V, Mirebeau I and Baldinozzi G 2000 *Phys. Rev.* B **61** R11871
[26] Garcaña-Muñoz J L and Rodríguez-Carvajal J 1992 *Phys. Rev.* B **46** 4414
[27] Staub U, Meijer G I, Fauth F, Allenspach R, Bednorz J G, Karpinski J, Kazakov S M, Paolasini L and d'Acapito F 2002 *Phys. Rev. Lett.* **88** e126402
[28] Scagnoli V, Staub U, Janousch M, Mulders A M, Shi M, Meijer G I, Rosenkranz S, Wilkins S B, Paolasini L, Karpinski J, Kazakov S M and Lovesey S W 2005 *Phys. Rev.* B **72** 155111
[29] Mazin I I, Khomskii D I, Lengsdorf R, Alonso J A, Marshall W G, Ibberson R M, Podlesnyak A, Martnez-Lope M J and Abd-Elmeguid M M 2007 *Phys. Rev. Lett.* **98** 176406
[30] Jeng H-T, Guo G Y and Huang D J 2004 *Phys. Rev. Lett.* **93** 156403
[31] Leonov I, Yaresko A N, Antonov V N, Korotin M A and Anisimov V I 2004 *Phys. Rev. Lett.* **93** 146404
[32] Tokura Y and Nagaosa N 2000 *Science* **288** 462
[33] Blake G R, Palstra T T M, Ren Y, Nugroho A A and Menovsky A A 2001 *Phys. Rev. Lett.* **87** 245501
[34] Jeng H-T, Lin S-H and Hsue C-S 2006 *Phys. Rev. Lett.* **97** 067002